Electronic Supplementary Material (ESI) for Chemical Communications.

Supplementary Information

Promoted kinetics and capacity on the $Li_2CuTi_3O_8$/C anode by constructing a one dimensional hybrid structure for superior performance lithium ion batteries

Yakun Tang, Jian Liu, Yue Zhang, Wenjie Ma, Lang Liu*, Biao Zhang and Sen Dong

State Key Laboratory of Chemistry and Utilization of Carbon Based Energy Resources; College of Chemistry, Xinjiang University, Urumqi, 830017, Xinjiang, PR China.

Email: llyhs1973@sina.com; liulang@xju.edu.cn

Experimental Section

Synthesis

The synthesis process of $Li_2CuTi_3O_8$/C hybrid nanotubes is as follows. Firstly, 70 mg sulfonated polymer nanotubes (SPNTs) were dispersed in 4 mL ethanol under ultrasonication for 0.5 h. Secondly, 1.22 g tetrabutyltitanate (TBT) was added to the mixture and stirred for 12 h. Then, 0.2 g $LiNO_3$ and 0.46 g $Cu(NO_3)_2 \cdot 3H_2O$ were dispersed in 8 mL ethanol solution and added into the above system and stirred for 6 h at 60 °C. After centrifugation, the residue was wiped with tissue paper to remove the excess liquid. The obtained solid was dried. Finally, the as-synthesized precursor was calcined at 900 °C for 6 h in N_2 (heating rate: 5 °C min^{-1}) to obtain $Li_2CuTi_3O_8$/C porous hybrid nanotubes (denoted LC). The synthesis path of sample LC is shown in Scheme S1.

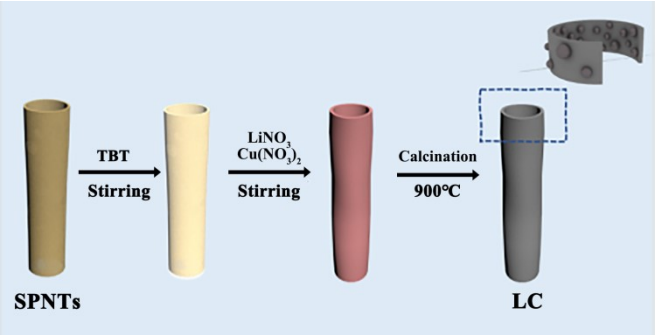

Scheme. S1 Fabrication process of the $Li_2CuTi_3O_8$/C porous hybrid nanotubes (LC).

Characterization

Morphologies and structure features of the samples were studied by using field emission scanning electron microscope (FESEM Hitachi S-4800) and high resolution transmission electron microscope (HRTEM JEOL JEM-2010F). Phase composition of the samples was characterized with X-ray diffraction (XRD, Bruker D8 advance with

Cu Ka radiation). Thermogravimetric analysis (TGA) was carried out with a Netzsch STA 449C at a heating rate of 10 ℃ min^{-1} from 30 to 800 ℃ in air. Nitrogen adsorption-desorption isotherms were recorded by using an Autosorb-iQ Pressure Sorption Analyzer (Quantachrome Instruments U. S.) at 77 K. The Brunauer-Emmett-Teller (BET) method was utilized to calculate the specific surface areas. Pore size distributions were calculated by the Density Functional Theory (DFT) method.

Electrochemical Characterization

2032 coin cells were used to measure electrochemical performances of the sample, with Li metal as the counter and reference electrodes. A slurry consisting of 80 wt% active materials, 10 wt% carbon black and 10 wt% poly (vinylidene fluoride) binder in N-methyl-2-pyrrolidone (NMP) was casted on a Cu foil, followed by drying at 110 ℃ over night in a vacuum oven. In an argon-filled glove box, celgard 2400 membrane was used as the separator and $LiPF_6$ (1 M) in ethylene carbonate/diethyl carbonate (1:1 vol) was employed as the electrolyte. Cyclic voltammograms (CVs) were collected on an electrochemical workstation (CHI660D, Chenhua, China) at a scan rate of 0.1 mV s^{-1}. Galvanostatic charge-discharge tests were performed on a Land (CT2001A China) between 0.01 and 3.00 V (versus Li^+/Li). Specific capacities were calculated based on the total mass of the composite material.

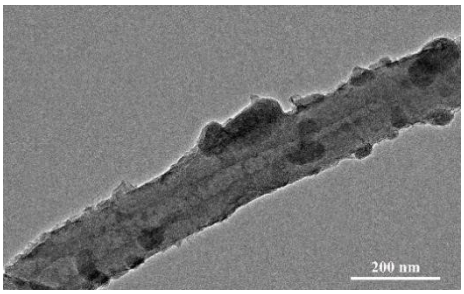

Fig. S1 TEM image of LC after 1000 cycles at 10 A g^{-1}.

Table. S1 Cycling performances and capacities of modified $Li_4Ti_5O_{12}$ compositions and

$Li_2ZnTi_3O_8$ based materials reported in the open literature.

Typical materials	Current density (mA g^{-1})	Cycle numbers	Remaining capacity (mAh g^{-1})	Tested condition (V)	Ref
$Li_4Ti_5O_{12}$@C	175	200	170	0.01-3.0	1
$Li_4Ti_5O_{12}$@C-Cu	1000	200	185	0.02-3.0	2
Cu-doped-$Li_4Ti_5O_{12}$	175	200	207.5	0.01-3.0	3
Fe-doped-$Li_4Ti_5O_{12}$	87.5	200	228.7	0-3.0	4
Al-doped-ZnO/$Li_4Ti_5O_{12}$	175	250	190	0.1-3.0	5
Nb-doped-$Li_2ZnTi_3O_8$	227	50	173.7	0.05-3.0	6
Mo-doped-$Li_2ZnTi_3O_8$	2000	200	147	0.02-3.0	7
N,C-doped-$Li_2ZnTi_3O_8/TiO_2$	1000	200	140.7	0.02-3.0	8
Cr-doped-$Li_2ZnTi_3O_8$	1000	200	162.2	0.05-3.0	9
$Li_2ZnTi_3O_8$@α-Fe_2O_3	1000	200	160	0-3.0	10
LC	200	200	402.8	0.01-3.0	this work
	2000	200	191.9	0.01-3.0	this work

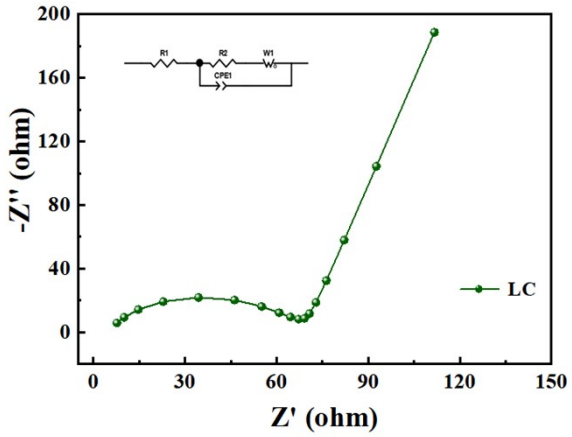

Fig. S2 Nyquist plot of LC.

Table S2. EIS fitting results of Ti-based spinel compositions.

Typical materials	$R_S(\Omega)$	$R_{ct}(\Omega)$	Ref
$Li_4Ti_5O_{12}$/PANI	11.2	109.4	R11
$Li_2ZnTi_3O_8$	6.176	138.7	R12
$Li_2COTi_3O_8$	6.5	192	R13
$Li_2Zn_{0.5}Cu_{0.5}Ti_3O_8$	7.525	96.33	R14
$Li_2CuTi_3O_8$	7.84	111.3	
$Li_2CuTi_3O_8$	11.99	110.6	
$Li_2MnTi_3O_8$	19.91	209.4	R15
$Li_2Cu_{0.5}Mn_{0.5}Ti_3O_8$	7.524	96.35	
LC	5.056	58.88	This work

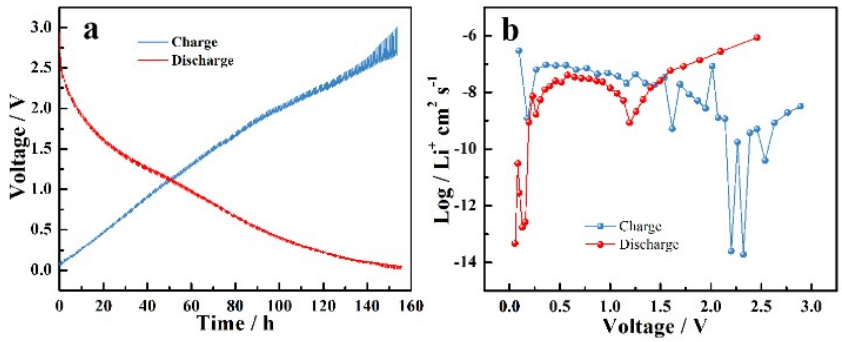

Fig. S3 Galvanostatic intermittent titration technique curves of LC for the charge and discharge process at 10 mA g^{-1} (a) and the chemical diffusion coeffcient of Li^+ as a function of voltage calculated from the GITT curves (b).

Table S3. Li^+ diffusion coefficient of spinel type materials reported in the literatures.

Typical materials	D_{Li+} (cm^2 s^{-1})	Ref
$Li_2CuTi_3O_8$	6.41E-14	R15
$Li_2MnTi_3O_8$	8.76E-15	
$Li_2Cu_{0.5}Mn_{0.5}Ti_3O_8$	4.79E-14	
$Li_4T_{i5}O_{12}$	3.30E-13	R16
$Li_4T_{i5}O_{12}$/Graphene	3.90E-10	R17
$Li_4Ti_5O_{12}/TiO_2$	7.66E-11	R18
$Li_4Ti_5O_{12}$/PANI	1.58E-12	R11

References

1. L. Y. Zheng, X. Y. Wang, Y. G. Xia, S. L. Xia, E. Metwalli, B. Qiu, Q. Ji, S. S. Yin, S. Xie, K. Fang, S. Z. Liang, M. M. Wang, X. X. Zuo, Y. Xiao, Z. P. Liu, J. Zhu, P. Müllery-Buschbaum and Y. J. Cheng, *ACS Appl. Mater. Interfaces.*, 2018, **10**, 2591-2602.
2. X. Bai, T. Li and Y. J. Bai, *ACS Sustain. Chem. Eng*., 2020, **8**, 17177-17184.
3. X. Q. Deng, W. R. Li, M. H. Zhu, D. P. Xiong and M. He, *Solid State Ionics*., 2021, **364**, 115614.
4. G. J. Yang and S. J. Park, *J. Mater. Chem. A.*, 2020, **8**, 2627-2636.
5. Y. Jin, H. Yu, Y. Gao, X. Q. He, T. A. White and X. H. Liang, *J. Power Sources.*, 2019, **436**, 226859.
6. N. Firdous, N. Arshad, S. B. Simonsen, P. Kadirvelayutham and P. Norby, *J. Power Sources.*, 2020, **462**, 228186.
7. S. Wang, Y. F. Bi, L. J. Wang, Z. H. Meng and B. M. Luo, *Electrochimi. Acta*, 2019, **301**, 319-324.
8. G. S. Sim, P. Santhoshkumar, J. W. Park, C. W. Ho, N. Shaji, H. K. Kim, M. Nanthagopal and C. W. Lee, *Ceram. Int*., 2021, **47**, 33554-33562.
9. X. G. Zeng, J. Peng, H. F. Zhu, Y. Gong and X. Huang, *Front. Chem*., 2020, **8**, 600204.
10. Y. Li, T. F. Yi, X. Z. Li, X. Q. Lai, J. J. Pan, P. Cui, Y. R. Zhu and Y. Xie, *Ceram. Int*., 2021, **47**, 18732-18742.
11. L. Y. Mo and H. T. Zheng, *Energy Rep*., 2020, **6**, 2913-2918.
12. C. Chen, C. C. Ai and X. Y. Liu, *Electrochimi. Acta.*, 2018, **265,** 448-454.
13. M. G. Fayed, S. G. Mohamed, Y. F. Barakat, E. E. EI-Shereafy and M. M. Rashad, *Bull. Mater Sci.*, 2022, **45**, 130.
14. W. Chen, H. F. Liang, W. J. Ren, L. Y. Shao, J. Shu and Z. C. Wang, *J. Alloys Compd.*, 2014, **611**, 65-73.
15. W. Chen, Z. R. Zhou, H. F. Liang, W. J. Ren, J. Shu and Z. C. Wang, *Mater. Chem. Phys.*, 2016, **169**, 128-135.
16. Y. Q. Feng, H. Liu, X. G. Zhao and W. W. Dong, *J. Phys. Chem. Solids.*, 2020, **146**, 109569.
17. F. Zhang, F. Y. Yi, A. M. Gao, D. Shu, Z. H. Sun, J. H. Mao, X. P. Zhou, Z. H. Zhu and Y. H. Sun, *J. Alloys Compd.*, 2020, **819**, 153018.
18. B. B. Pan, Z. Q. Zhao, P. Hu, Z. H. Zhang and Z. L. Huang, *Mater. Lett.*, 2021, **300**, 130166.